Electronic Supplementary Information for:

Fine Tune of the Charge Separated State Energy in Compact Orthogonal Naphthalene-Phenoxazine Dyads and Its Effect on the Thermally Activated Delayed Fluorescence

Jieyu Tang,‡[a] Xi Liu,‡[b] Xue Zhang,[a] Jianzhang Zhao*[a] and Yan Wan*[b]

[a] State Key Laboratory of Fine Chemicals, Frontiers Science Center for Smart Materials, School of Chemical Engineering, Dalian University of Technology, Dalian 116024, (P. R. China). *E-mail: zhaojzh@dlut.edu.cn (J.Z.)

[b] College of Chemistry, Beijing Normal University, Beijing 100875 (P. R. China). *E-mail: wanyan@bnu.edu.cn

Contents

1. Experimental Section ..... Page S3

2. Synthesis of the Compounds ..... Page S3

3. Molecular Structure Characterization Data ..... Page S6

4. Crystallographic Data ..... Page S12

5. Steady State UV–vis Absorption ..... Page S13

6. Fluorescence Emission Spectra ..... Page S15

7. Fluorescence Lifetimes ..... Page S19

8. Cyclic Voltammograms ..... Page S23

9. Nanosecond Transient Absorption Spectroscopy ..... Page S24

10. Femtosecond Transient Absorption Spectroscopy ..... Page S27

11. Calculated by DFT and TDDFT with Gaussian 16 ..... Page S29

12. Computed Electronic Transitions ..... Page S30

13. Reference ..... Page S30

1. Experimental Section

General Information. All the chemicals used in synthesis are analytically pure and were used as received. Solvents in reaction were dried prior to use. ^{1}H and ^{13}C NMR spectra were recorded on the Bruker Avance spectrometers (400 MHz). ^{1}H and ^{13}C chemical shifts are reported in parts per million (ppm) relative to TMS, with the residual solvent peak used as an internal reference. The mass spectra were measured by HRMS (ESI). UV-vis absorption spectra were measured on a UV-2550 spectrophotometer (Shimadzu Ltd., Japan).

2. Synthesis of the Compounds

2.1. The synthesis of compounds **NI-Br-Bu**, **NI-Br-Ph**, **NI-Br-PhF**, **NI-Br-PhOCH$_3$**, and **NI-PXZ-Bu**[1] have been reported.

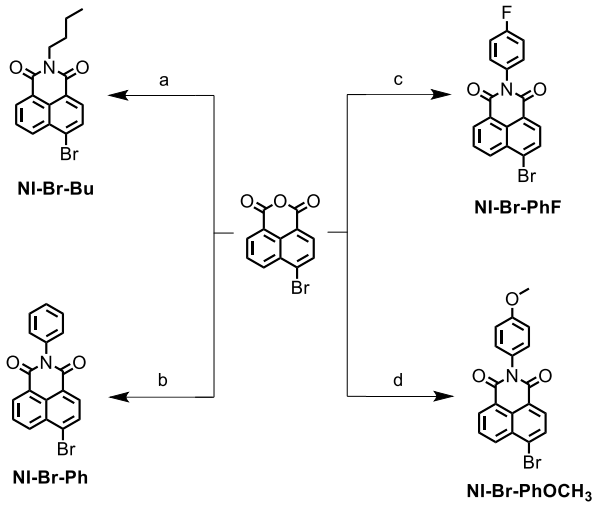

Scheme S1. Synthesis of the Dyads. (a) n-Butylamine, 4-Bromo-1,8-naphthalic anhydride, ethanol, 80°C, 32%; (b) Aniline, 4-Bromo-1,8-naphthalic anhydride, CH_3COOH, 120°C, 89%; (c) 4-Fluoroaniline, 4-Bromo-1,8-naphthalic anhydride, CH_3OH, 70°C, 90%; (d) p-Anisidine, 4-Bromo-1,8-naphthalic anhydride, CH_3COOH, 120°C, 82%.

2.2. Synthesis of NI-Br-Ph, NI-Br-PhF, NI-Br-PhOCH$_3$.[2]

NI-Br-Ph Aniline (251 mg, 2.70 mmol) and 4-Bromo-1,8-naphthalic anhydride (500 mg, 1.80 mmol) were added with acetic acid (CH_3COOH, 21 mL), heated to 120°C, and stirred for 20 h hours. The reaction was cooled to room temperature and the solvent was removed by rotary evaporation under reduced pressure. The obtained crude product was purified by column chromatography (silica gel as the stationary phase and dichloromethane as the eluent) to give a pale yellow solid. Yield: 634 mg, 89%. ^{1}H NMR ($CDCl_3$, 400 MHz): δ(ppm) = 8.59 (t, 2H, *J* = 7.00 Hz), 8.34 (d, 1H, *J* = 7.80 Hz), 8.25 (d, 1 H, *J* = 7.90 Hz), 8.03 (t, 1H, *J* = 7.90 Hz), 7.53 (t, 2H, *J* = 7.20 Hz), 7.48 (d, 1H, *J* = 7.00 Hz), 7.39 (d, 2H, *J* = 7.20 Hz).

NI-Br-PhF 4-Fluoroaniline (1.74 mL, 18.4 mmol), 4-Bromo-1,8-naphthalic anhydride (502 mg, 1.81 mmol) were dissolved in CH_3OH (21 mL). The reaction was stirred at 70°C for 12 hours. The crude product was washed with deionized water, the ethanol was removed by suction filtration, and dried under vacuum for 4 h to obtain a yellow-brown solid. Yield: 556 mg, 90%. ^{1}H NMR ($CDCl_3$, 400 MHz): δ(ppm) = 8.74 (d, 1H, *J*=7.20 Hz), 8.67 (d, 1H, *J*=8.50 Hz), 8.48 (d, 1H, *J*=7.80 Hz), 8.11 (d, 1H, *J*=7.90 Hz,), 7.94 – 7.90 (m, 1H), 7.33 – 7.29 (m, 2H), 7.25 (d, 2H, *J*=8.80 Hz,).

NI-Br-PhOCH$_3$ p-Anisidine (838 mg, 2.20 mmol), 4-Bromo-1,8-naphthalic anhydride (503 mg, 1.82 mmol), were added with CH_3COOH, heated to 120°C. The reaction was stirred for 12 hours, and the crude product was purified by column chromatography using silica gel as the stationary phase and dichloromethane as the eluent to obtain a pale yellow solid. Yield: 568 mg, 82%. ^{1}H NMR ($CDCl_3$, 400 MHz) δ(ppm) = 8.71 (d, 1H, *J* = 8.30 Hz), 8.64 (d, 1H, *J* = 8.50 Hz), 8.46 (d, 1H, *J* = 7.90 Hz), 8.08 (d, 1H, *J* = 7.90 Hz), 7.93 – 7.85 (m, 1H), 7.23 (d, 2H, *J* = 8.90 Hz), 7.06 (d, 2H, *J* = 8.90 Hz), 3.88 (s, 3H).

2.3. Synthesis of NI-PXZ-Bu.[3]

NI-PXZ-Bu NI-Br-Bu (66 mg, 0.20 mmol), phenoxazine (44 mg, 0.24 mmol), cesium carbonate (78 mg, 0.24 mmol), cuprous iodide (3.80 mg, 0.02 mmol) were added with N,N-

Dimethylformamide (DMF), (3 mL), and the mixture was heated to 120°C with stirring under nitrogen for 12 hours. After cooling, water was added, and the mixture was extracted with dichloromethane (DCM). The organic layers were combined and washed with water and brine solution, respectively. The organic layer was dried over anhydrous Na_2SO_4 and the solvent was evaporated under reduced pressure. and the organic phases were combined. The obtained red crude product was purified by column chromatography (silica gel. dichloromethane: n-hexane = 2:1, v/v) to obtain a black-red solid. Yield: 24 mg, 29%. Mp: 235.3–236.7 °C. ^{1}H NMR (400 MHz, $CDCl_3$) δ(ppm) = 8.79 (d, 1H, *J*=7.70 Hz,), 8.66 (d, 1H, *J*=7.30 Hz), 8.43 (d, 1H, *J*=8.40 Hz), 7.84 (d, 1H, *J*=7.70 Hz), 7.76 – 7.72 (m, 1H), 6.79 (d, 2H, *J*=7.00 Hz), 6.68 – 6.71 (m, 2H), 6.54 – 6.50 (m, 2H), 5.69 (d, 2H, *J*=7.90 Hz,), 4.23 (t, 2H, *J*=7.60 Hz), 1.79 – 1.72 (m, 2H), 1.53 – 1.44 (m, 2H), 1.00 (t, 3H, *J*=7.30 Hz). HRMS (ESI): calcd for $C_{28}H_{23}N_2O_3$ $[M+H]^+$, *m*/*z* 435.1709; found: *m*/*z* 435.1696.

3. Molecular Structure Characterization Data

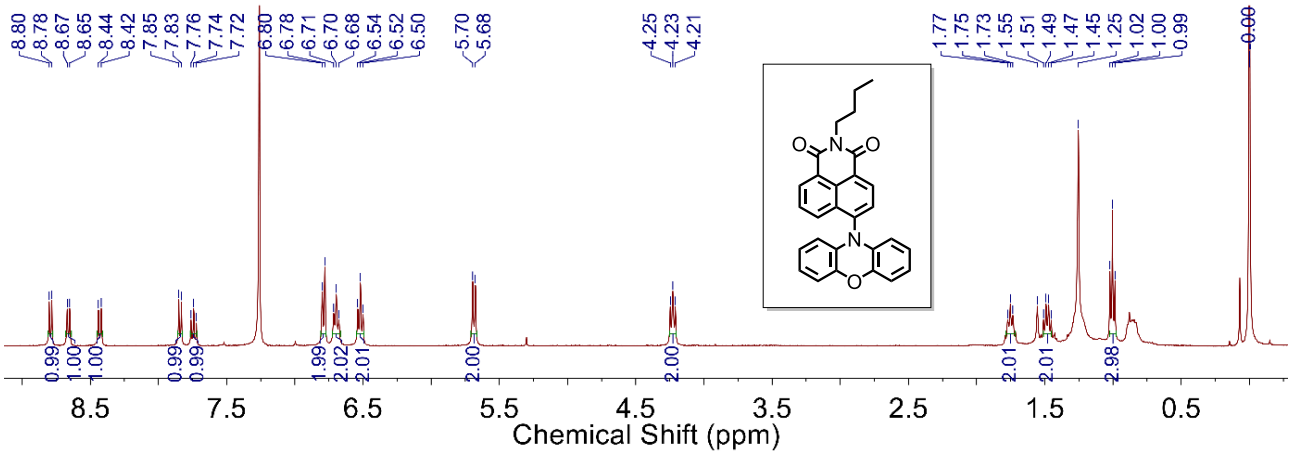

Figure S1. ^{1}H NMR spectra of **NI-PXZ-Bu** (400 MHz, $CDCl_3$)

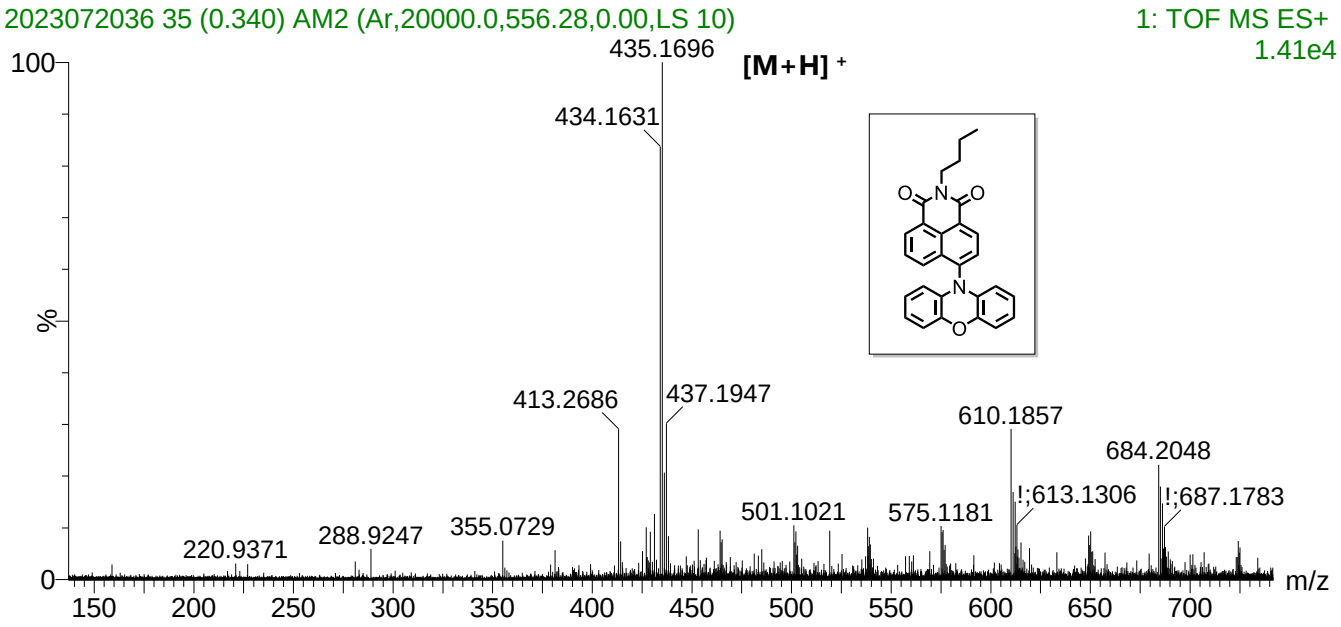

Figure S2. ESI-HRMS of **NI-PXZ-Bu**

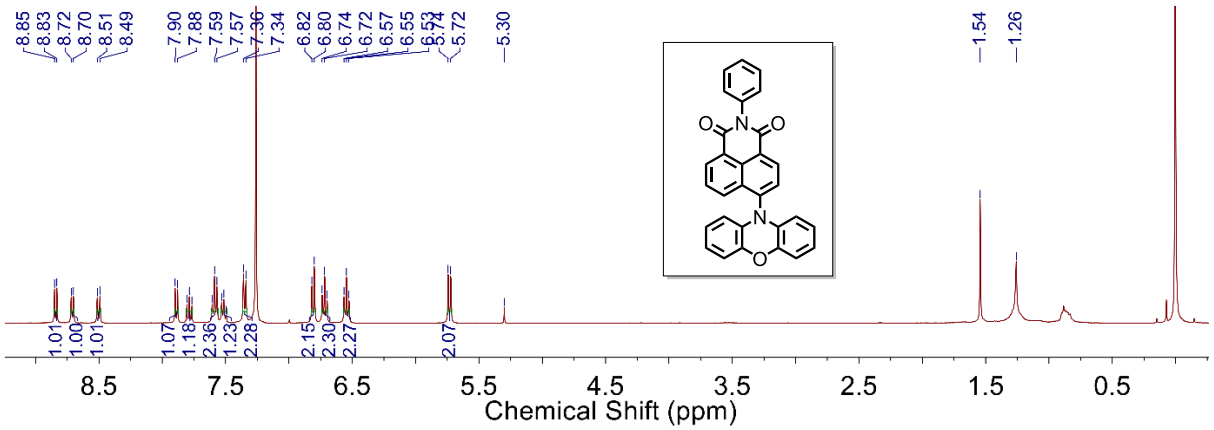

Figure S3. ^{1}H NMR spectra of **NI-PXZ-Ph** (400 MHz, $CDCl_3$)

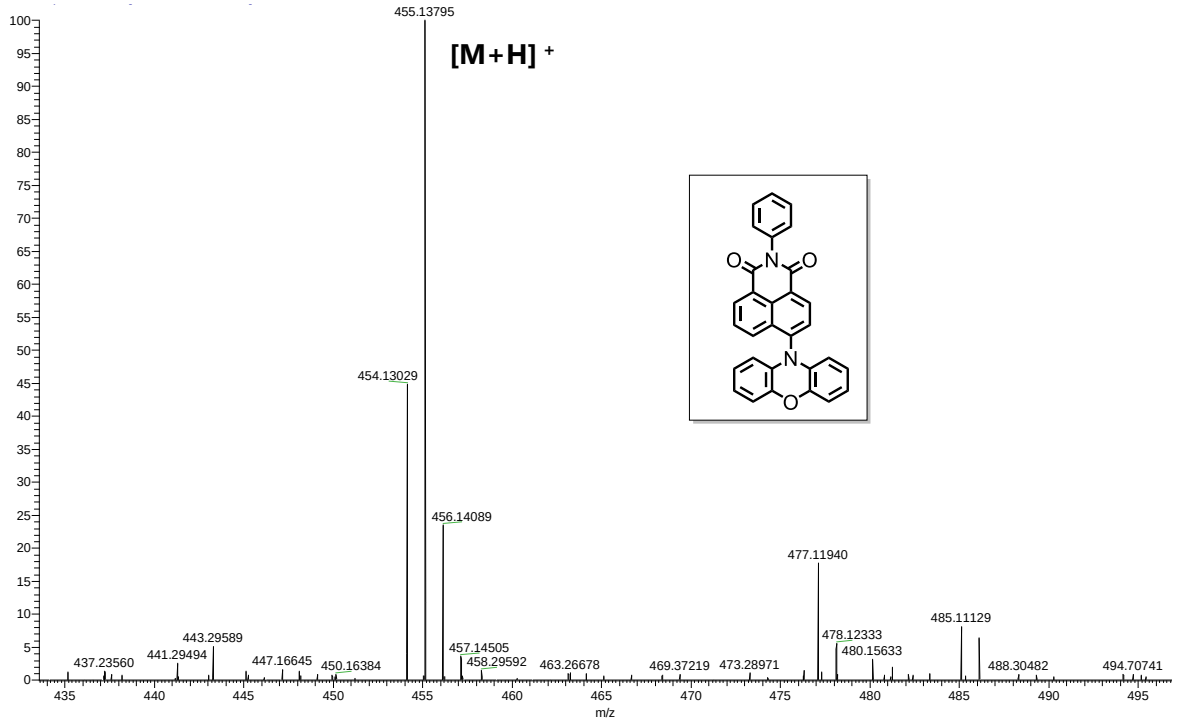

Figure S4. ESI-HRMS of **NI-PXZ-Ph**

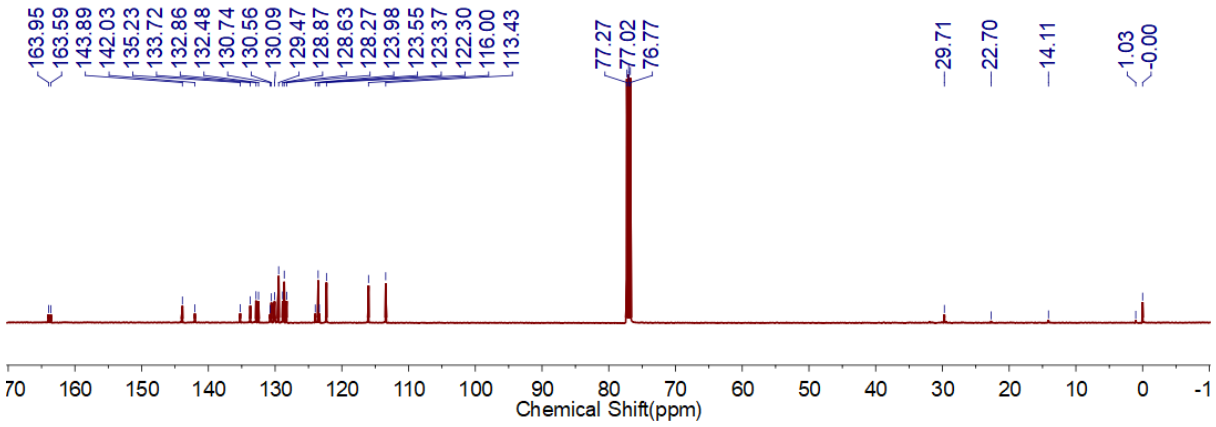

Figure S5. ^{13}C NMR spectrum of compound **NI-PXZ-Ph** ($CDCl_3$, 126 MHz)

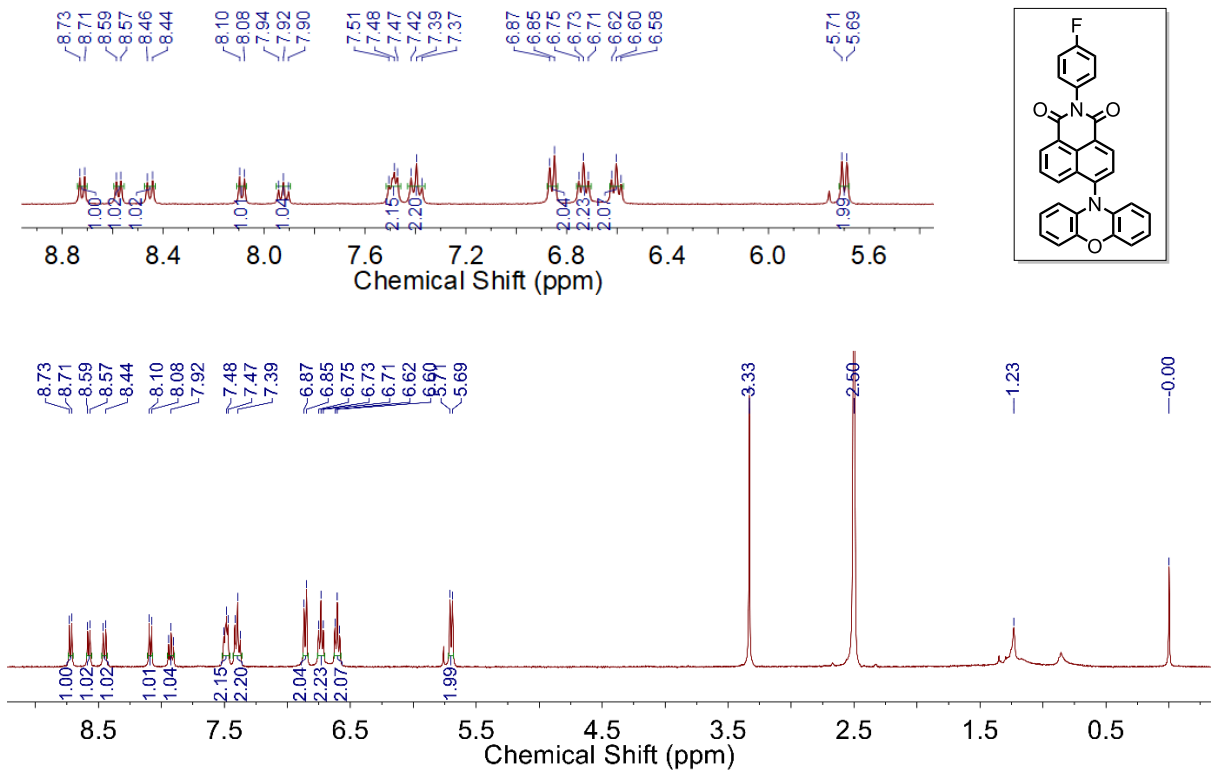

Figure S6. ^{1}H NMR spectra of **NI-PXZ-PhF** (400 MHz, DMSO-d_6)

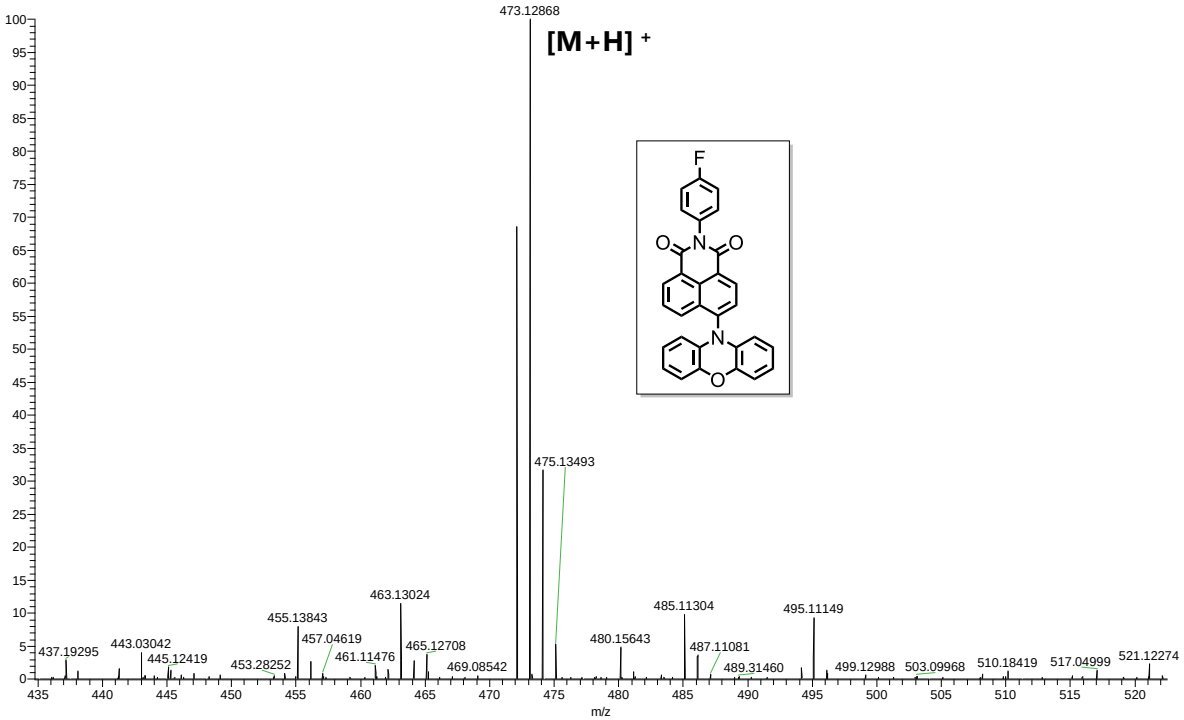

Figure S7. ESI-HRMS of **NI-PXZ-PhF**

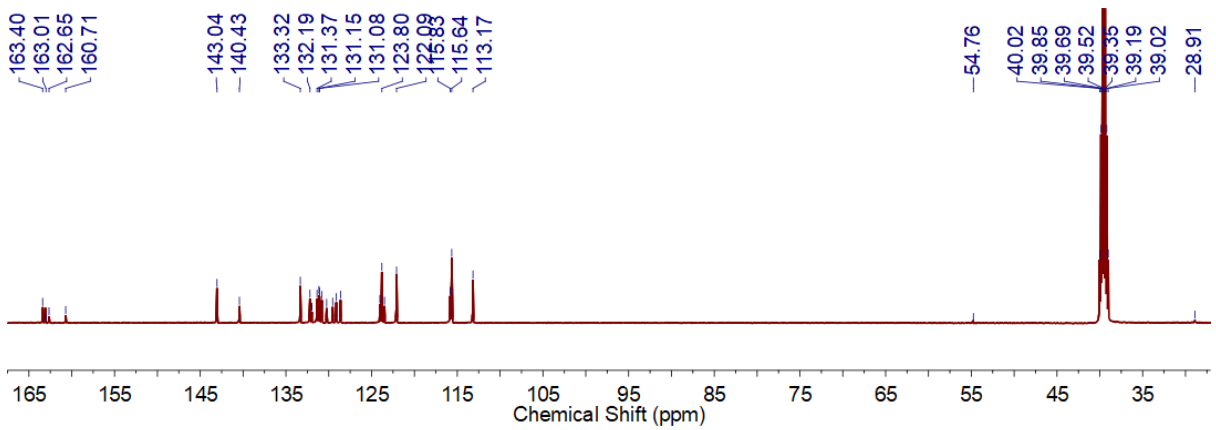

Figure S8. ^{13}C NMR spectrum of compound **NI-PXZ-PhF** (DMSO-d_6, 126 MHz)

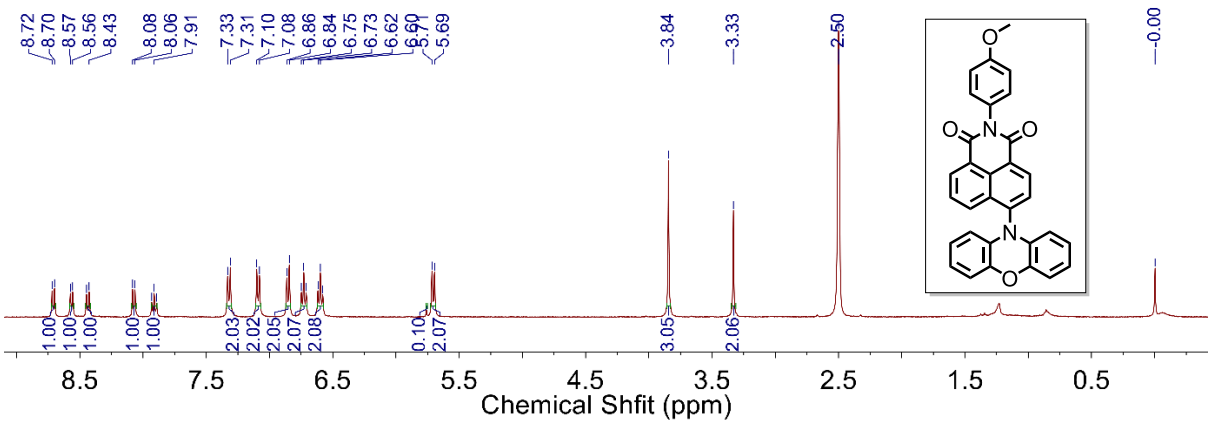

Figure S9. ^{1}H NMR spectra of **NI-PXZ-PhOCH$_3$** (400 MHz, DMSO-d_6)

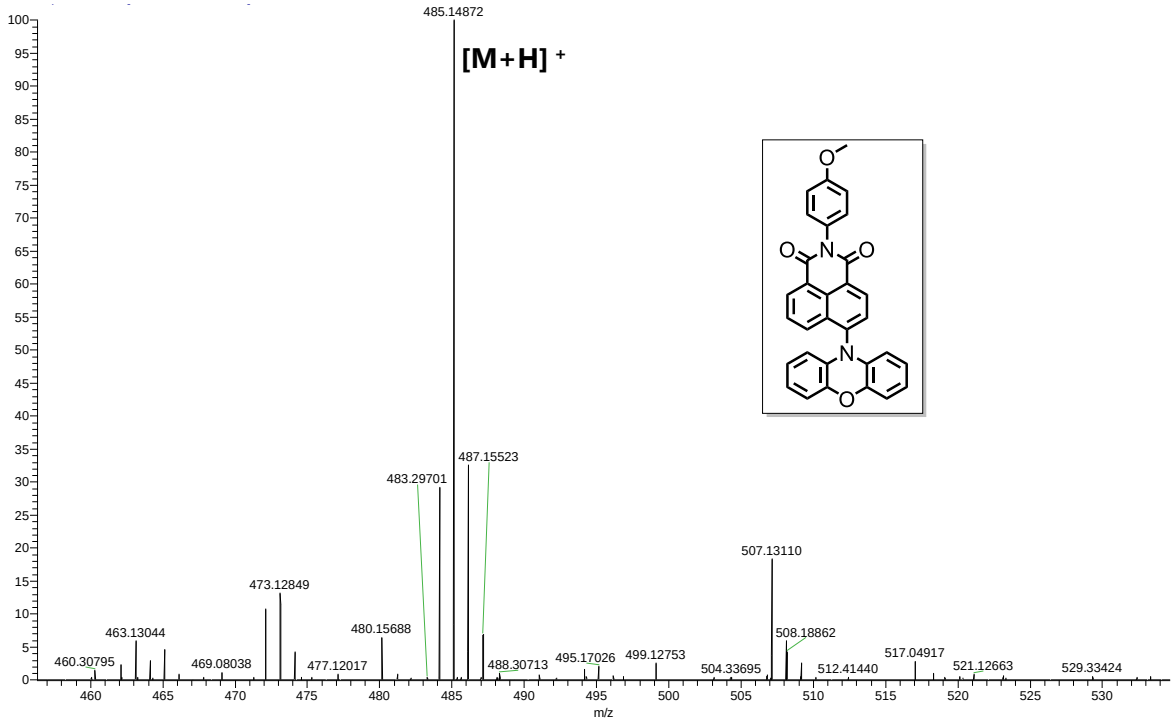

Figure S10. ESI-HRMS of **NI-PXZ- PhOCH$_3$**

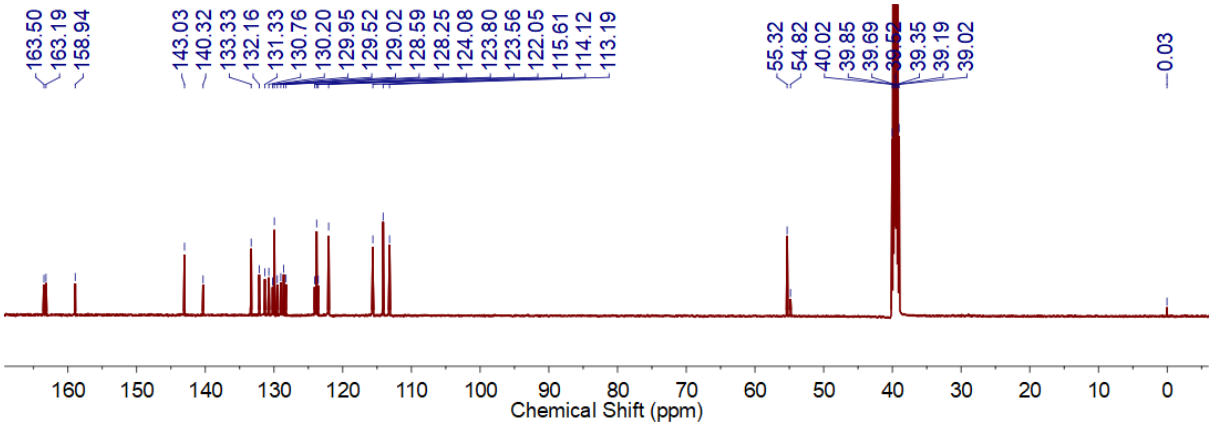

Figure S11. ^{13}C NMR spectrum of compound **NI-PXZ-PhOCH$_3$** (DMSO-d_6, 126 MHz)

4. Crystallographic Data

Table S1. Crystallographic Data for **NI-PXZ**. [a]

Compound	**NI-PXZ-Ph**	**NI-PXZ-PhF**	**NI-PXZ-PhOCH$_3$**
Sum formula	$C_{30}H_{18}N_2O_3$	$C_{30}H_{17}FN_2O_3$	$C_{31}H_{19}N_2O_4$
M (g mol^{-1})	454.46	472.45	483.48
Temperature / K	273.7	298	294.8
Crystal system	orthorhombic	orthorhombic	monoclinic
Space group	$P2_12_12_1$	$P2_12_12_1$	$P2_1/n$
a (Å)	12.7810(7)	12.5160(6)	8.6346(8)
b (Å)	12.8680(6)	12.9592(7)	22.406(3)
c (Å)	13.2627(7)	13.5707(8)	12.3194(14)
α (deg)	90	90	90
β (deg)	90	90	105.684(3)
γ (deg)	90	90	90
Volume / Å^3	2181.26(19)	2201.1(2)	2294.7(4)
Z	4	4	4
D_{calc} / g · cm^{-3}	1.384	1.426	1.399
F (000)	944.0	976.0	1004.0
μ (Mo − Kα) / mm^{-1}	0.090	0.099	0.094
θ_{max} (deg)	24.724	25.056	25.016
Reflections collected	24469	12319	16901
Independent reflections	3716 [R_{int} = 0.0643, R_{sigma} = 0.0400]	3832 [R_{int} = 0.0632, R_{sigma} = 0.0621]	4021 [R_{int} = 0.0964, R_{sigma} = 0.0909]
Parameters	316	393	333
Largest diff. peak and hole (e Å^{-3})	0.14/-0.16	0.12/-0.14	0.56/-0.43
Goodness of fit	1.070	1.040	1.042
R^a	0.0427	0.0435	0.1254
$wR_2{}^a$	0.1050	0.1091	0.2784

[a] $\boldsymbol{R} = \sum \big||\boldsymbol{F_0}| - |\boldsymbol{F_C}|\big| / \sum |\boldsymbol{F_0}|$, $\boldsymbol{\omega R_2} = \left[\sum \boldsymbol{\omega}(|\boldsymbol{F_0}|^2 - |\boldsymbol{F_c}|^2) / \sum \boldsymbol{\omega}\left(\boldsymbol{F_0^2}\right)^2\right]^{1/2}$, $[F_0 > 4\sigma(F_0)c^2]$

After repeated refinement, the wR_2 value is slightly larger, which is caused by poor crystal quality or weak diffraction points.

5. Steady State UV–vis Absorption

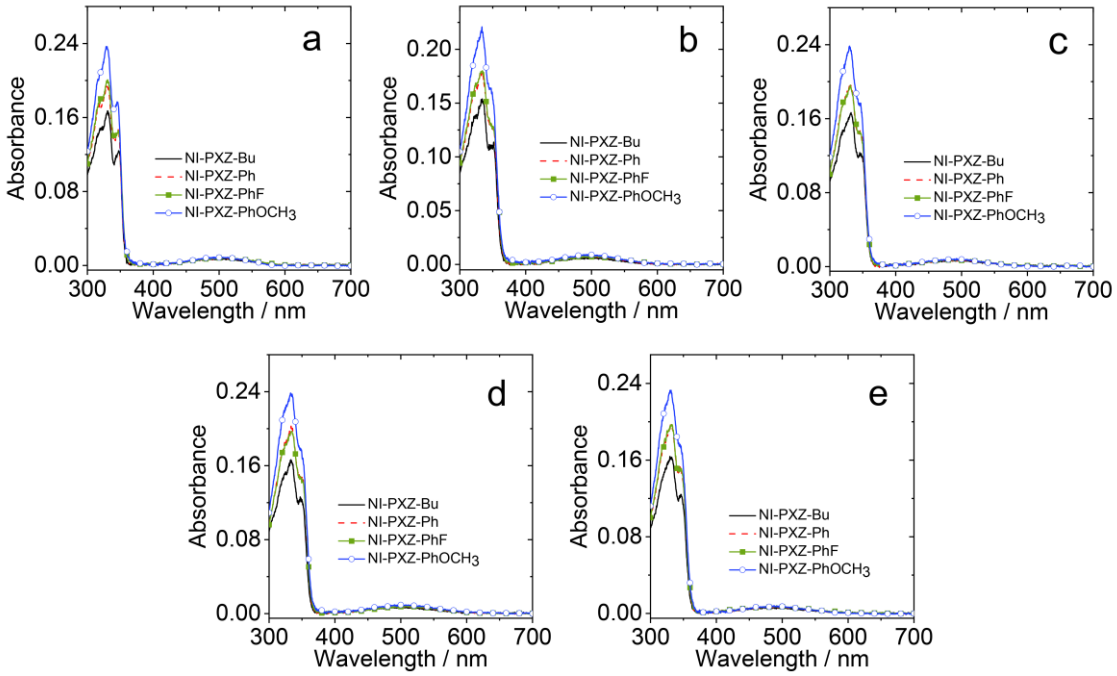

Figure S12. UV-vis absorption spectra of the compounds in (a) cyclohexane (CHX); (b) toluene (TOL); (c) tetrahydrofuran (THF); (d) dichloromethane (DCM) and (e) acetonitrile (ACN). *c* = 1.0×10^{-5} M, 25°C.

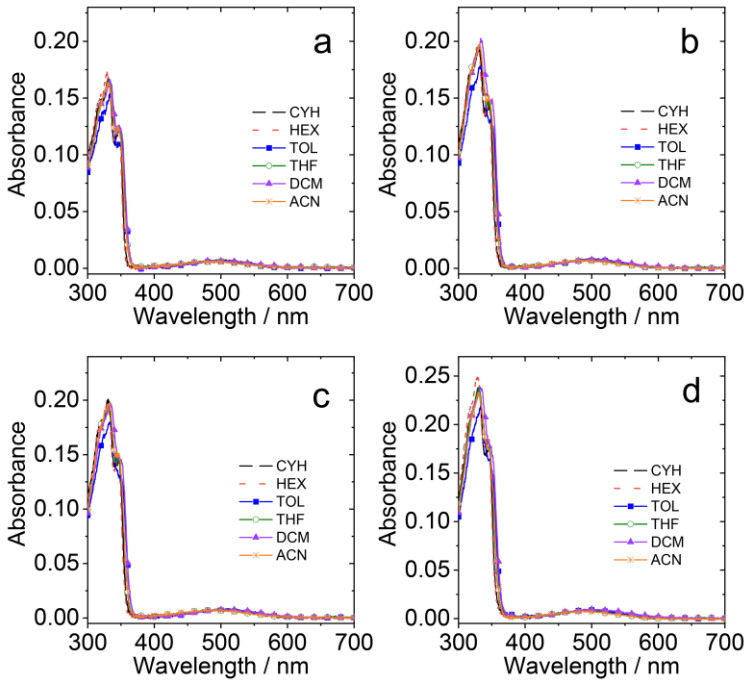

Figure S13. UV-vis absorption spectra of (a) **NI-PXZ-Bu**, (b) **NI-PXZ-Ph**, (c) **NI-PXZ-PhF** and (d) **NI-PXZ-PhOCH$_3$** in different solvents. $c = 1.0 \times 10^{-5}$ M, 25°C.

6. Fluorescence Emission Spectra

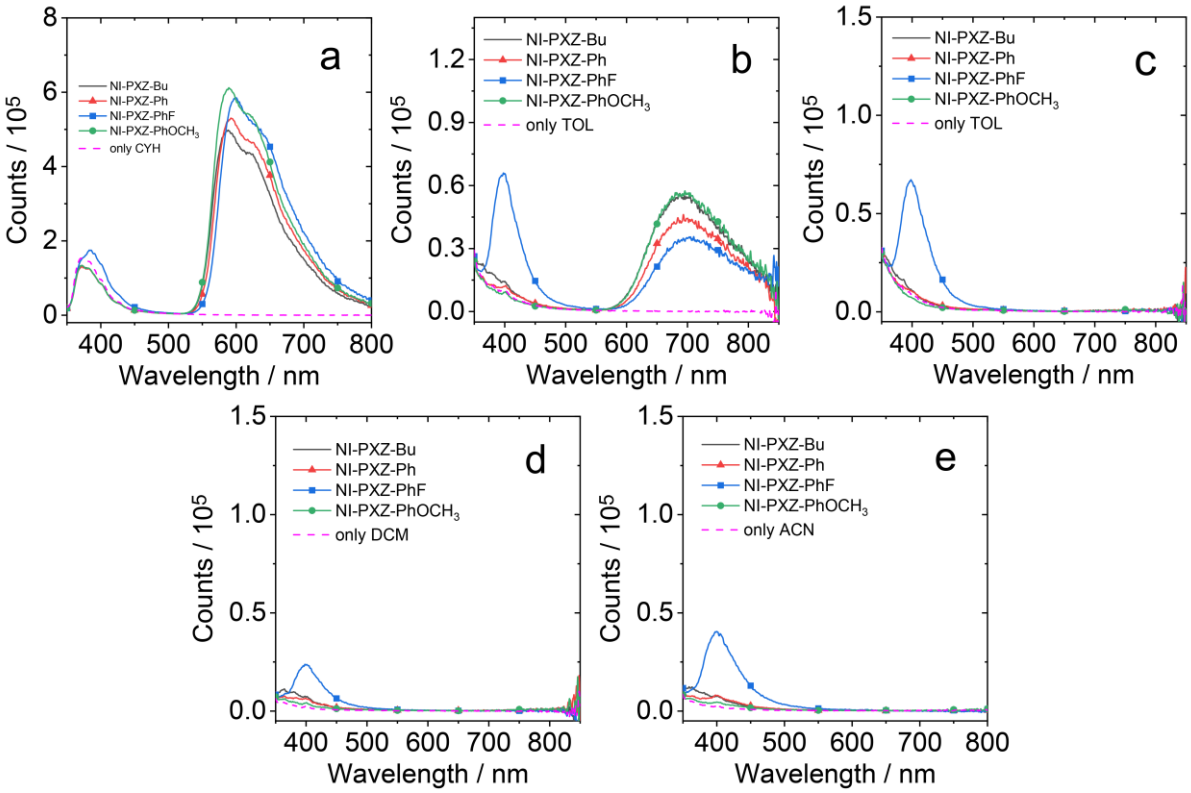

Figure S14. Comparison of the fluorescence spectra of the compounds in (a) CHX; (b) TOL; (c) THF; (d) DCM and (e) ACN. Optically matched solutions were used (A= 0.102 at λ_{ex} = 310 nm), 25°C.

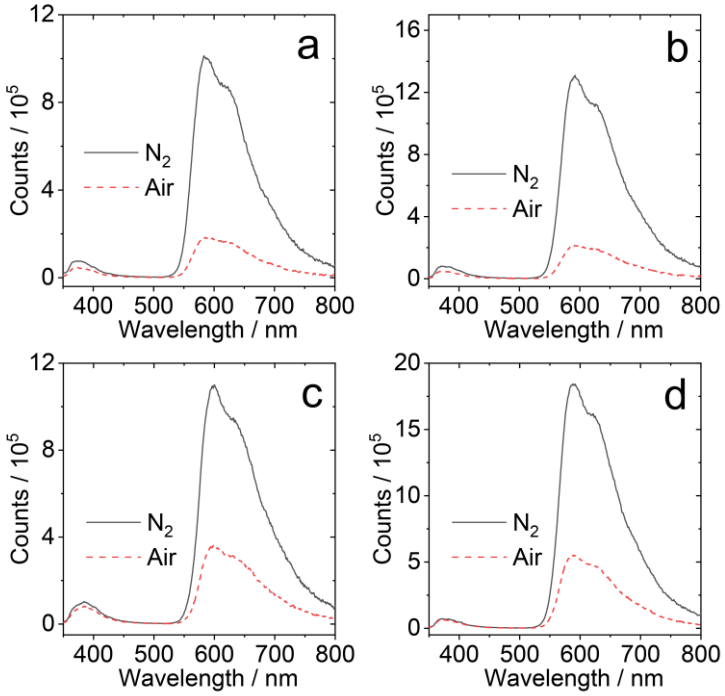

Figure S15. Fluorescence spectra of (a) **NI-PXZ-Bu**, (b) **NI-PXZ-Ph**, (c) **NI-PXZ-PhF** and (d) **NI-PXZ-PhOCH$_3$** in CHX. c= 1.0 ×10^{-5} M, λ_{ex} = 310 nm, 25 °C.

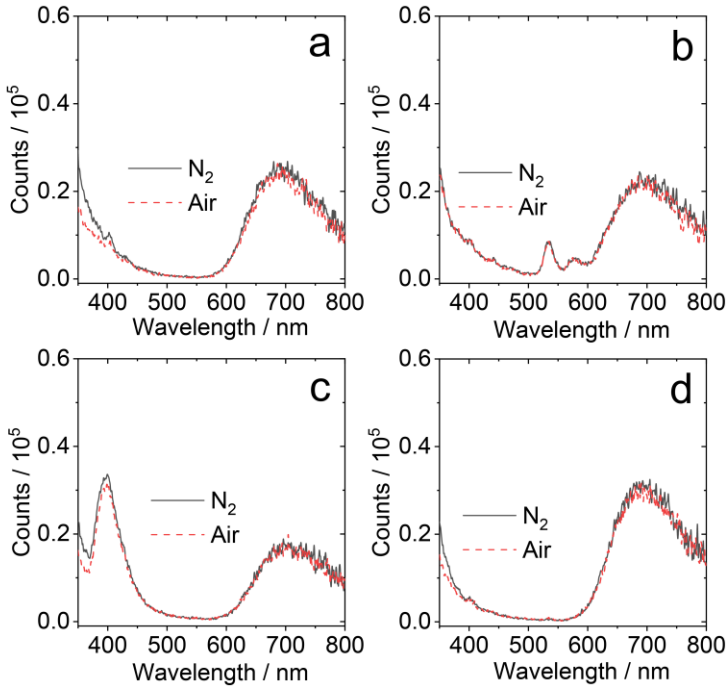

Figure S16. Fluorescence spectra of (a) **NI-PXZ-Bu**, (b) **NI-PXZ-Ph**, (c) **NI-PXZ-PhF** and (d) **NI-PXZ-PhOCH$_3$** in TOL. c= 1.0 ×10^{-5} M, λ_{ex} = 310 nm, 25 °C.

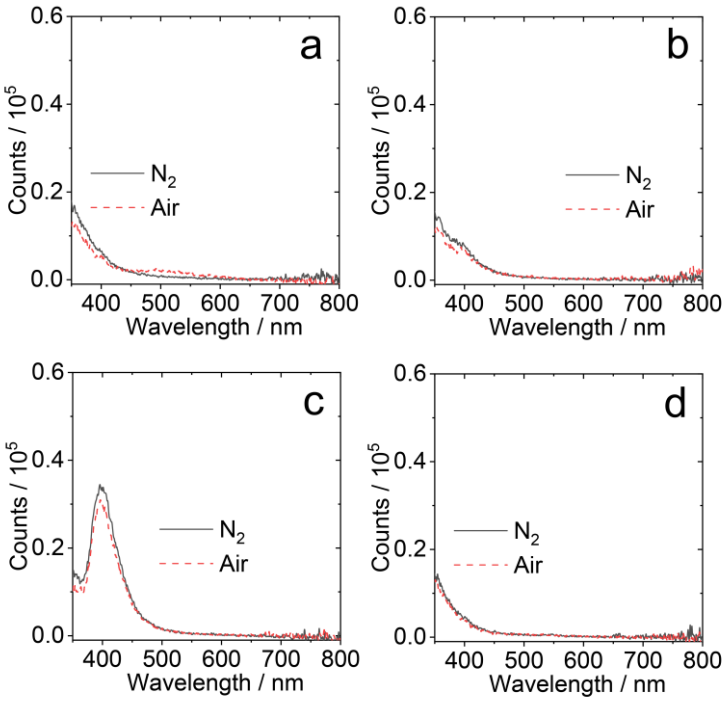

Figure S17. Fluorescence spectra of (a) **NI-PXZ-Bu**, (b) **NI-PXZ-Ph**, (c) **NI-PXZ-PhF** and (d) **NI-PXZ-PhOCH$_3$** in THF. c= 1.0 ×10^{-5} M, λ_{ex} = 310 nm, 25 °C.

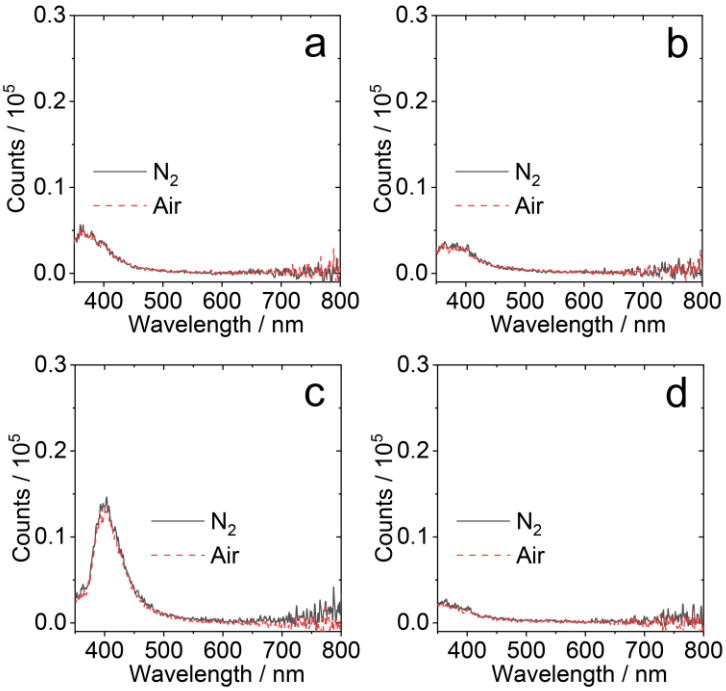

Figure S18. Fluorescence spectra of (a) **NI-PXZ-Bu**, (b) **NI-PXZ-Ph**, (c) **NI-PXZ-PhF** and (d) **NI-PXZ-PhOCH$_3$** in DCM. c= 1.0 ×10^{-5} M, λ_{ex} = 310 nm, 25 °C.

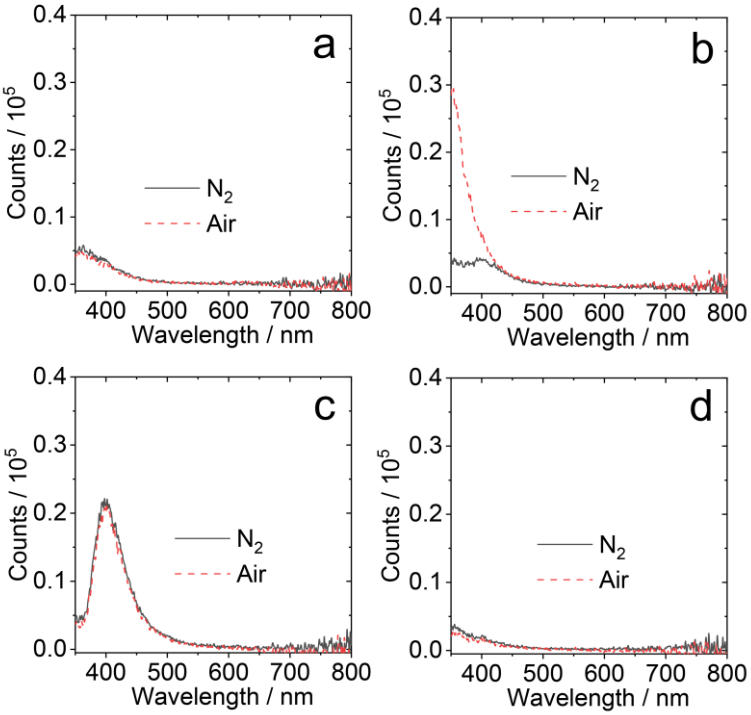

Figure S19. Fluorescence spectra of (a) **NI-PXZ-Bu**, (b) **NI-PXZ-Ph**, (c) **NI-PXZ-PhF** and (d) **NI-PXZ-PhOCH$_3$** in ACN. c= 1.0 ×10^{-5} M, λ_{ex} = 310 nm, 25 °C.

7. Fluorescence Lifetimes

Table S2. Fluorescence lifetimes of **NI-PXZ-Bu**, **NI-PXZ-Ph**, **NI-PXZ-PhF** and **NI-PXZ-PhOCH$_3$** under different atmosphere in CHX (i.e. before and after deoxygenation).

		τ_1/ns		τ_2/ns	
NI-PXZ-Bu	Nitrogen	17.48	99.1%	11730.0	0.9%
	Air	11.02	98.4%	329.3	1.6%
NI-PXZ-Ph	Nitrogen	19.74	98.9%	7674.0	1.1%
	Air	11.33	98.4%	346.6	1.6%
NI-PXZ-PhF	Nitrogen	21.24	99.0%	4867	1.0%
	Air	11.66	97.0%	317.3	3.0%
NI-PXZ-PhOCH$_3$	Nitrogen	18.71	98.9%	9317.0	1.1%
	Air	11.09	98.8%	340.6	1.2%

Excited at 340 nm (Picosecond pulsed diode laser) and monitored at 590 nm. c= 1.0 × 10^{-5} M in CHX, 25°C

Table S3. Fluorescence lifetimes of **NI-PXZ-Bu**, **NI-PXZ-Ph**, **NI-PXZ-PhF** and **NI-PXZ-PhOCH$_3$** under different atmosphere in HEX (i.e. before and after deoxygenation).

		τ_1/ns		τ_2/ns	
NI-PXZ-Bu	Nitrogen	16.47	99.3%	15960.0	0.7%
	Air	6.997	98.4%	256.8	1.6%
NI-PXZ-Ph	Nitrogen	18.51	99.3%	10620.0	0.7%
	Air	8.323	98.0%	236.9	2.0%
NI-PXZ-PhF	Nitrogen	20.24	99.2%	6375	0.8%
	Air	8.345	97.0%	261.5	3.0%
NI-PXZ-PhOCH$_3$	Nitrogen	16.80	99.3%	14000	0.7%
	Air	7.585	99.0%	272.6	1.0%

Excited at 340 nm (Picosecond pulsed diode laser) and monitored at 590 nm. c= 1.0 × 10^{-5} M in HEX, 25°C

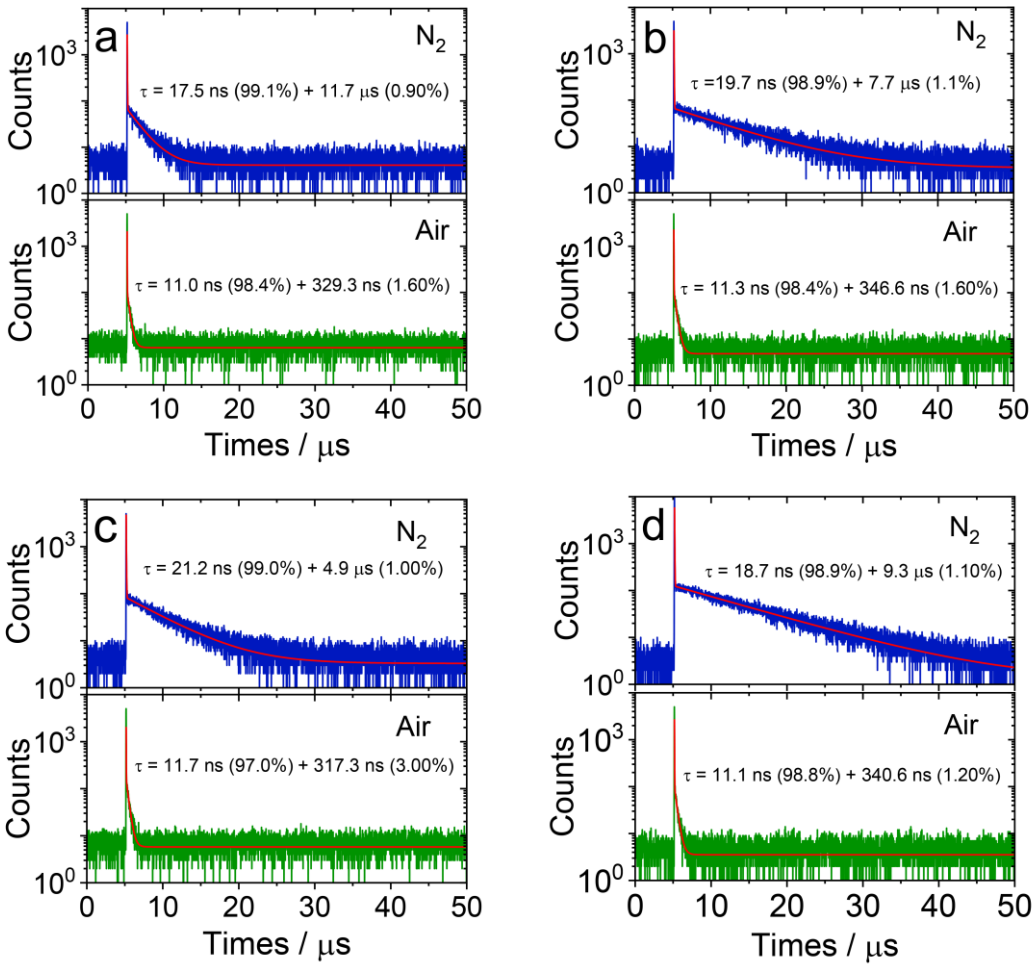

Figure S20. Fluorescence decay traces of (a) **NI-PXZ-Bu**, (b) **NI-PXZ-Ph**, (c) **NI-PXZ-PhF** and (d) **NI-PXZ-PhOCH$_3$** under different atmospheres (N_2, Air). λ_{ex} = 340 nm, decay trace at 590 nm. c = 1.0 × 10^{-5} M in cyclohexane, 25°C.

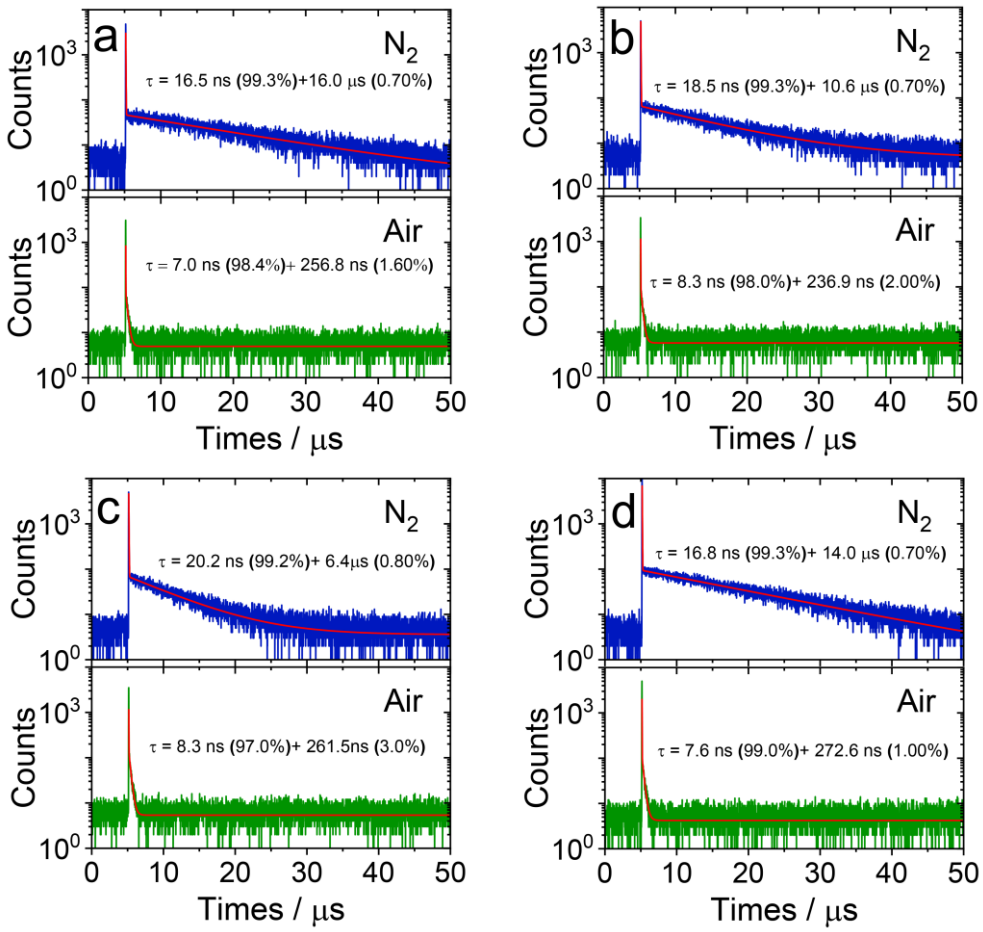

Figure S21. Fluorescence decay traces of (a) **NI-PXZ-Bu**, (b) **NI-PXZ-Ph**, (c) **NI-PXZ-PhF** and (d) **NI-PXZ-PhOCH$_3$** under different atmospheres (N_2, Air). λ_{ex} = 340 nm, decay trace at 590 nm. $c = 1.0 \times 10^{-5}$ M in *n*-hexane, 25°C.

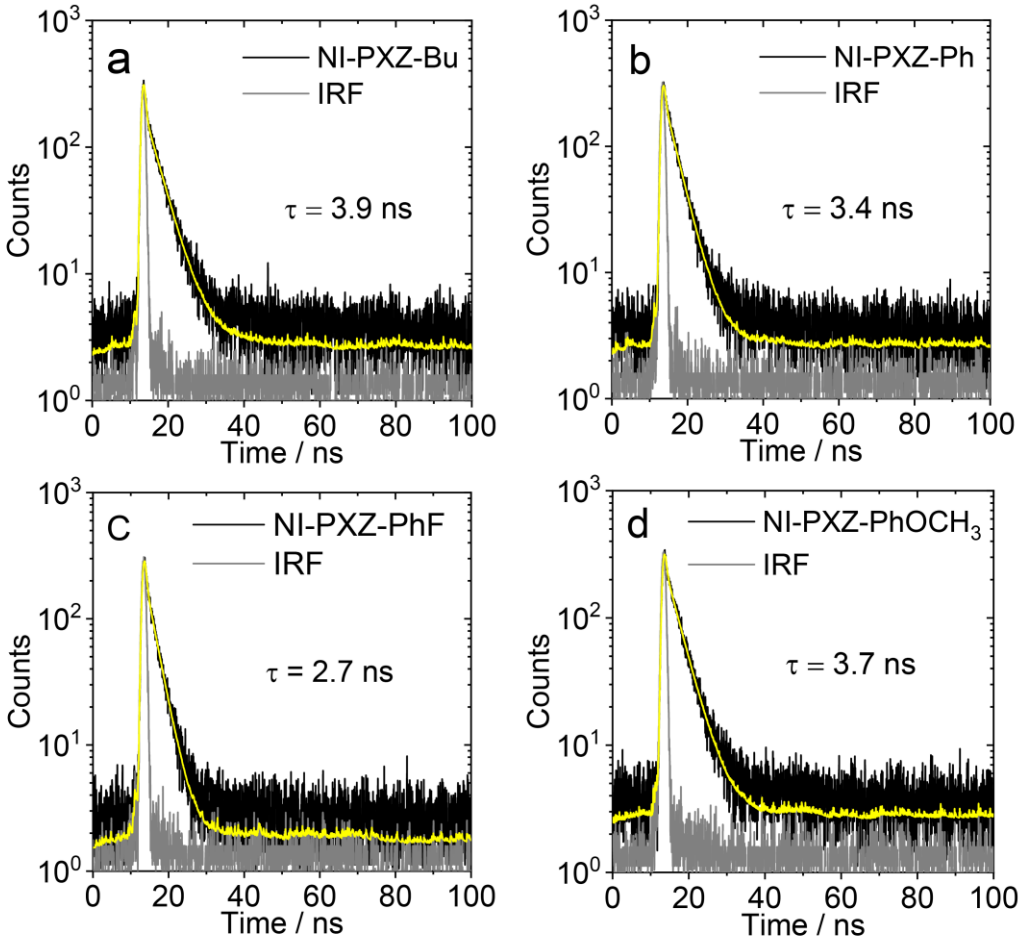

Figure S22. Fluorescence decay traces of (a) **NI-PXZ-Bu**, (b) **NI-PXZ-Ph**, (c) **NI-PXZ-PhF** and (d) **NI-PXZ-PhOCH₃** under N_2. λ_{ex} = 340 nm, decay trace at 710 nm. $c = 5.0 \times 10^{-5}$ M in toluene, 25°C.

8. Cyclic Voltammograms

Table S4. Redox Potentials of the Compounds[a]

Compounds	E_{RED} /V	E_{OX} /V	E_{HOMO}/eV[b]	E_{LUMO}/eV[c]	E_{CSS}(eV)[d]
NI-PXZ-Bu	−1.54	0.61	−5.41	−3.26	2.25
NI-PXZ-Ph	−1.50	0.61	−5.41	−3.3	2.23
NI-PXZ-PhF	−1.49	0.60	−5.40	−3.31	2.20
NI-PXZ-PhOCH$_3$	−1.51	0.61	−5.41	−3.29	2.24

[a] Cyclic voltammetry in N_2 saturated DCM containing a 0.10 M Bu_4NPF_6 supporting electrolyte; Counter electrode is Pt electrode; working electrode is glassy carbon electrode; Ag/$AgNO_3$ couple as the reference electrode. [b] Calculated by $E_{HOMO} = -4.78 + (E_{ox}(Fc) - E_{ox})$, [c] Calculated by $E_{LUMO} = -4.78 + (E_{ox}(Fc) - E_{RED})$. [d] The *E*css value obtained from the experimental value: *E*css = $1240/\lambda_{00}$ (λ_{00} is the intersection of CT absorption spectrum and CT emission spectrum in *n*-hexane. In nm).

9. Nanosecond Transient Absorption Spectroscopy

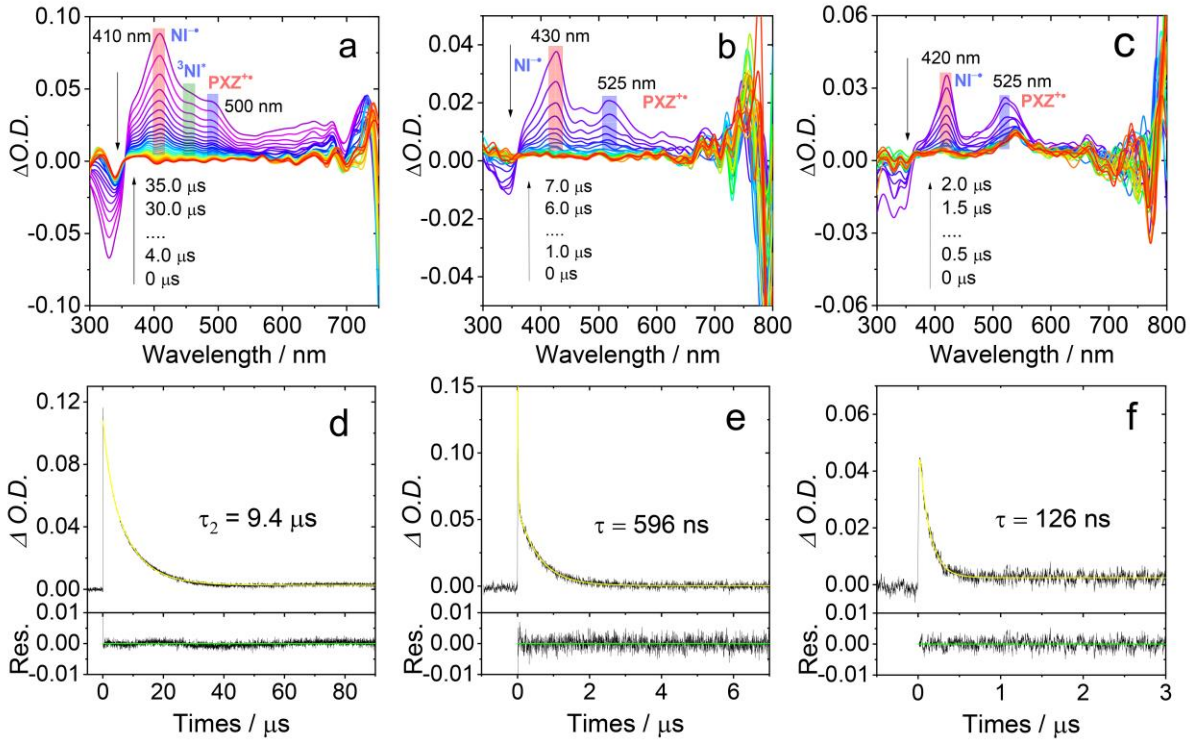

Figure S23. Nanosecond transient absorption spectra of **NI-PXZ-Bu** in (a) n-hexane, (b) toluene, (c) acetonitrile and decay curves at 410 nm in (d) n-hexane, (e) toluene (430 nm) and (f) acetonitrile (420 nm). Pulsed laser excitation at 355 nm, $c = 3.0 \times 10^{-5}$ M, 25°C.

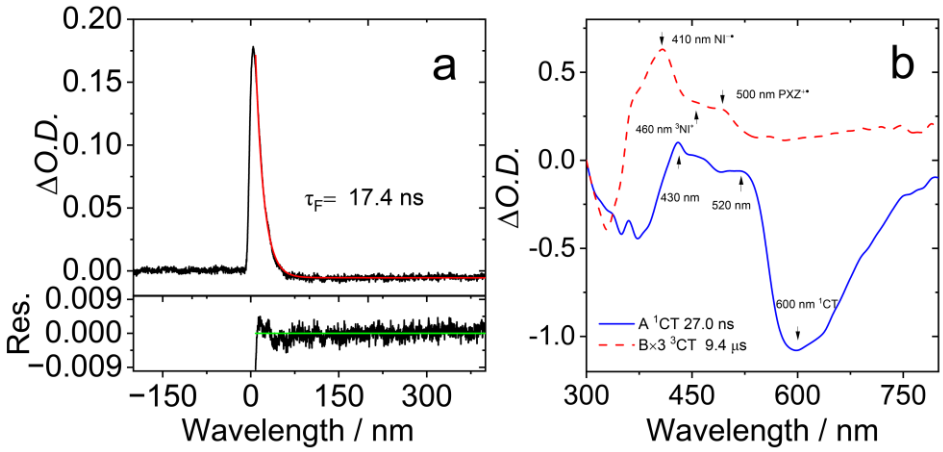

Figure S24. Nanosecond transient absorption spectra of **NI-PXZ-Bu** in *n*-hexane in short delay time range. Pulsed laser excitation at 355 nm $c = 3.0 \times 10^{-5}$ M, 25°C. (a) decay trace at 600 nm (b) EADS of the ns-TA spectra of the mixture upon laser excitation.

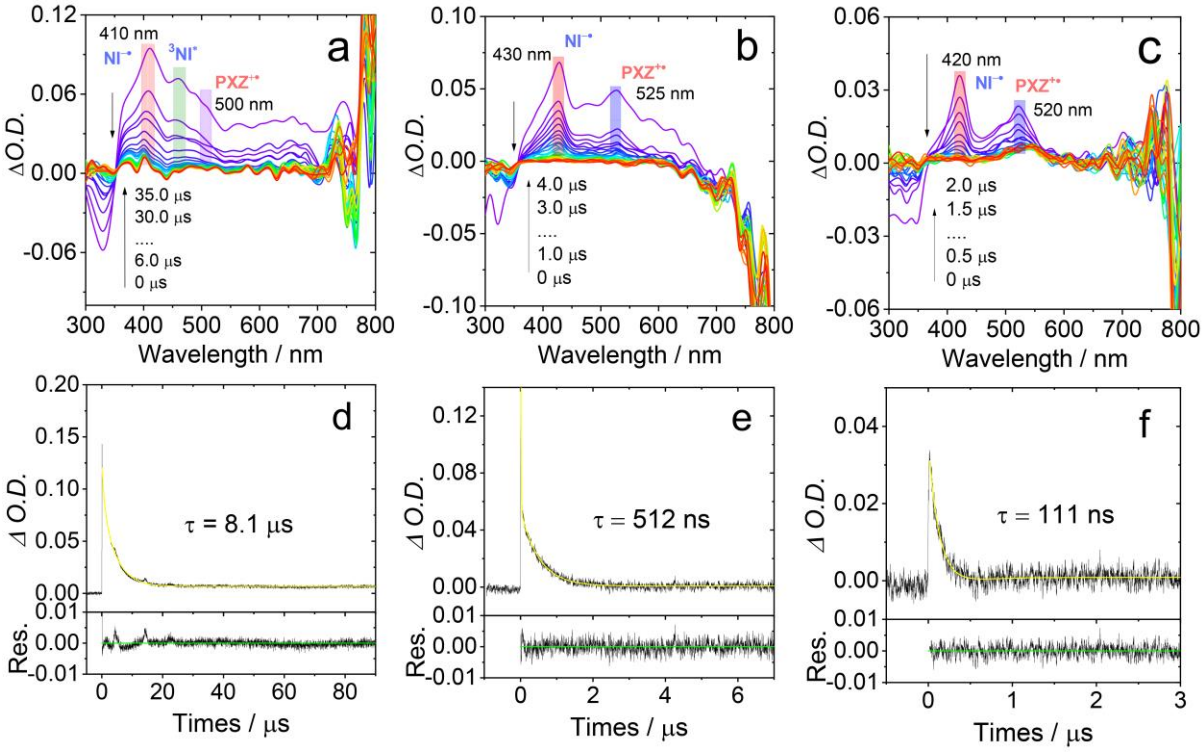

Figure S25. Nanosecond transient absorption spectra of **NI-PXZ-Ph** in (a) n-hexane, (b) toluene, (c) acetonitrile and decay curves at 410 nm in (d) n-hexane, (e) toluene (430 nm) and (f) acetonitrile (420 nm). Pulsed laser excitation at 355 nm, $c = 3.0 \times 10^{-5}$ M, 25°C.

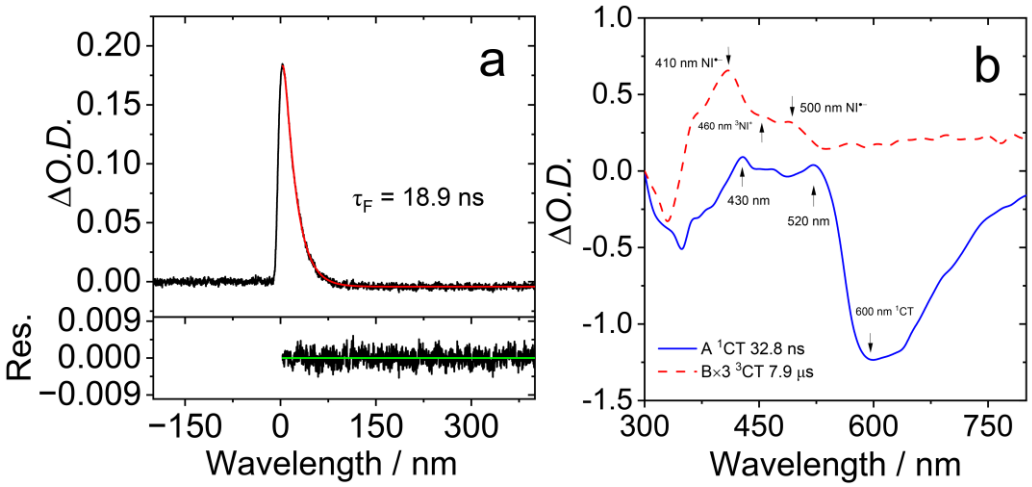

Figure S26. Nanosecond transient absorption spectra of **NI-PXZ-Ph** in *n*-hexane in short delay time range. Pulsed laser excitation at 355 nm $c = 3.0 \times 10^{-5}$ M, 25°C. (a) decay trace at 600 nm (b) EADS of the ns-TA spectra of the mixture upon laser excitation.

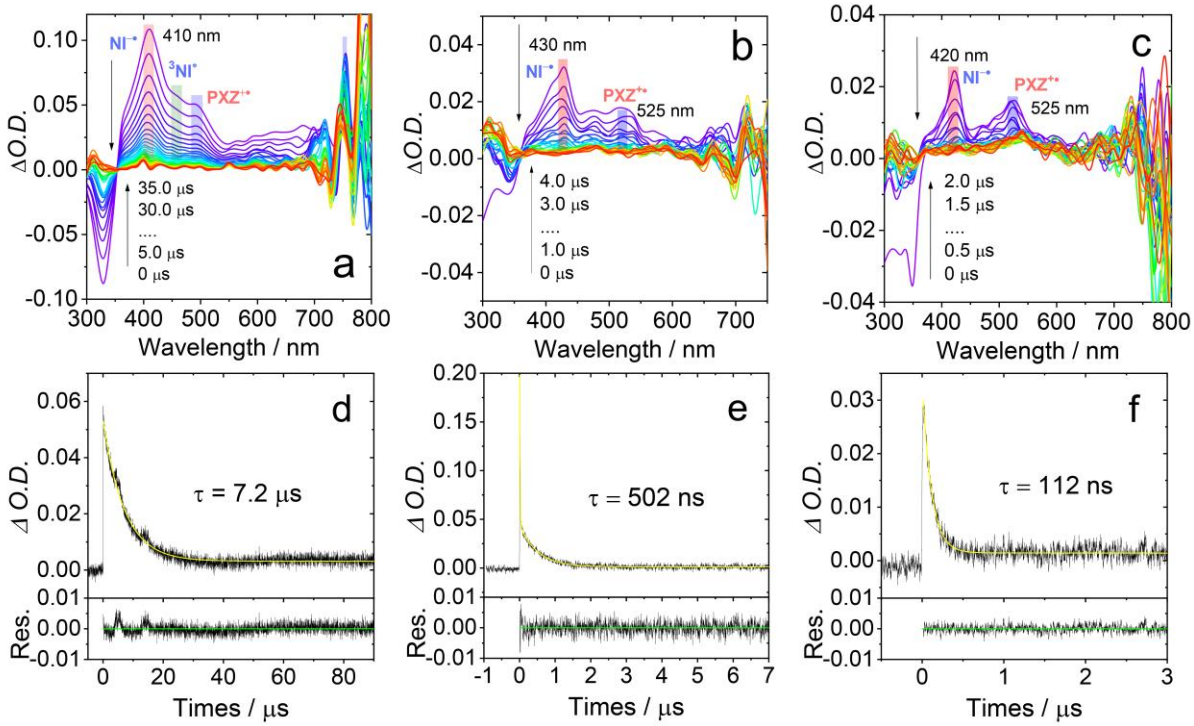

Figure S27. Nanosecond transient absorption spectra of **NI-PXZ-PhOCH$_3$** in (a) n-hexane, (b) toluene, (c) acetonitrile and decay curves at 410 nm in (d) n-hexane, (e) toluene (430 nm) and (f) acetonitrile (420 nm). Pulsed laser excitation at 355 nm, c = 3.0 × 10^{-5} M, 25°C.

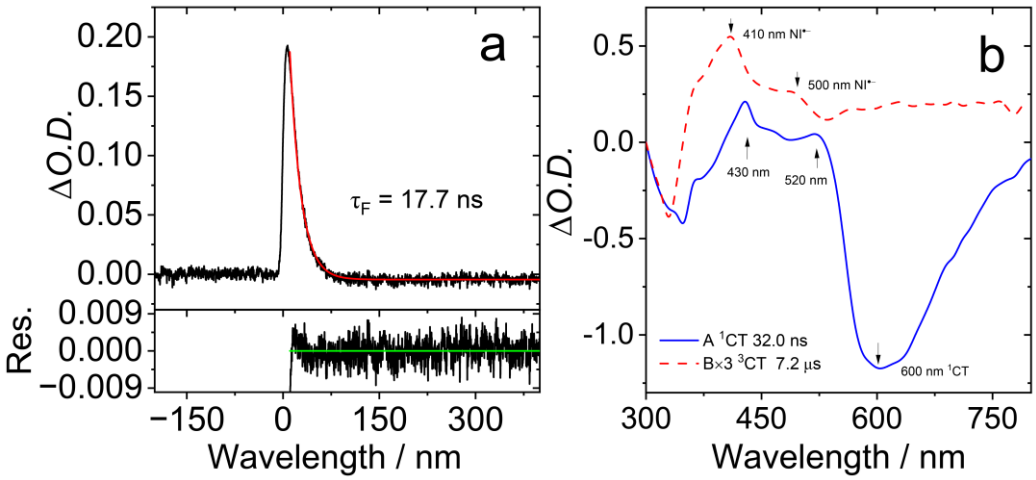

Figure S28. Nanosecond transient absorption spectra of **NI-PXZ-PhOCH$_3$** in *n*-hexane in short delay time range. Pulsed laser excitation at 355 nm c = 3.0 × 10^{-5} M, 25°C. (a) decay trace at 600 nm (b) EADS of the ns-TA spectra of the mixture upon laser excitation.

10. Femtosecond Transient Absorption Spectroscopy

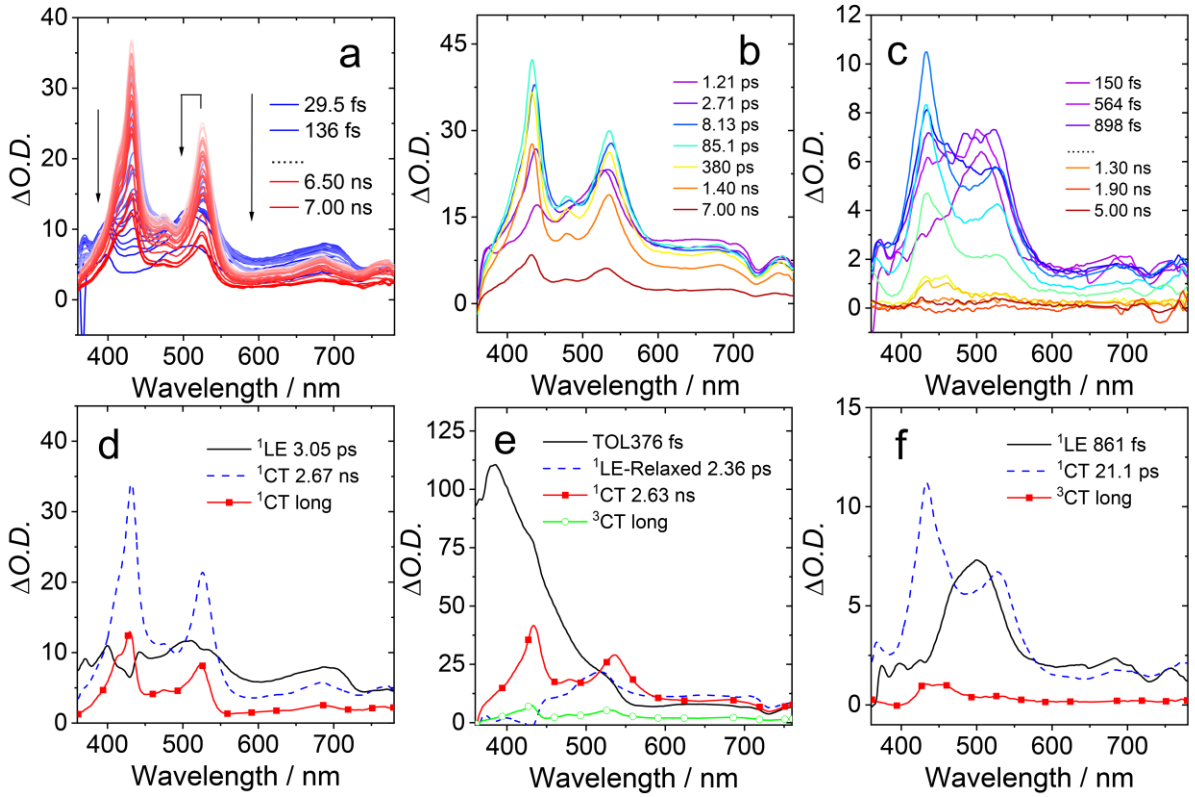

Figure S29. Femtosecond transient absorption spectra of **NI-PXZ-Bu** in (a) HEX, (b) TOL, (c) ACN and relative EADS obtained with global analysis of **NI-PXZ-Bu** in (d) HEX, (e) TOL, (f) ACN. Excited at 330 nm.

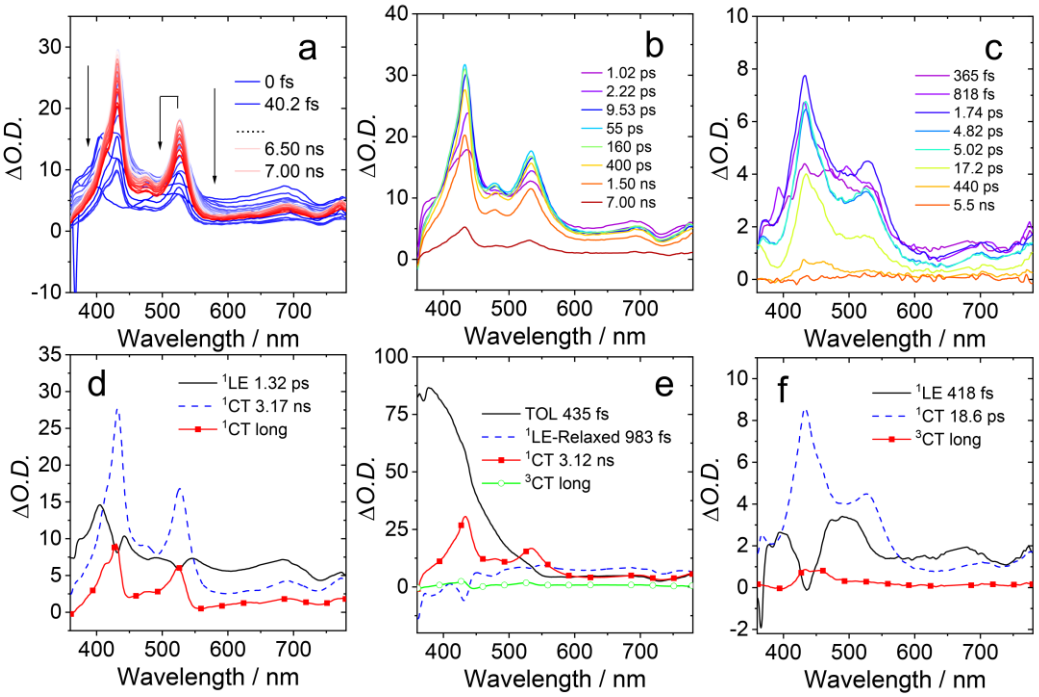

Figure S30. Femtosecond transient absorption spectra of **NI-PXZ-Ph** in (a) HEX, (b) TOL, (c) ACN and relative EADS obtained with global analysis of **NI-PXZ-Ph** in (d) HEX, (e) TOL, (f) ACN. Excited at 330 nm.

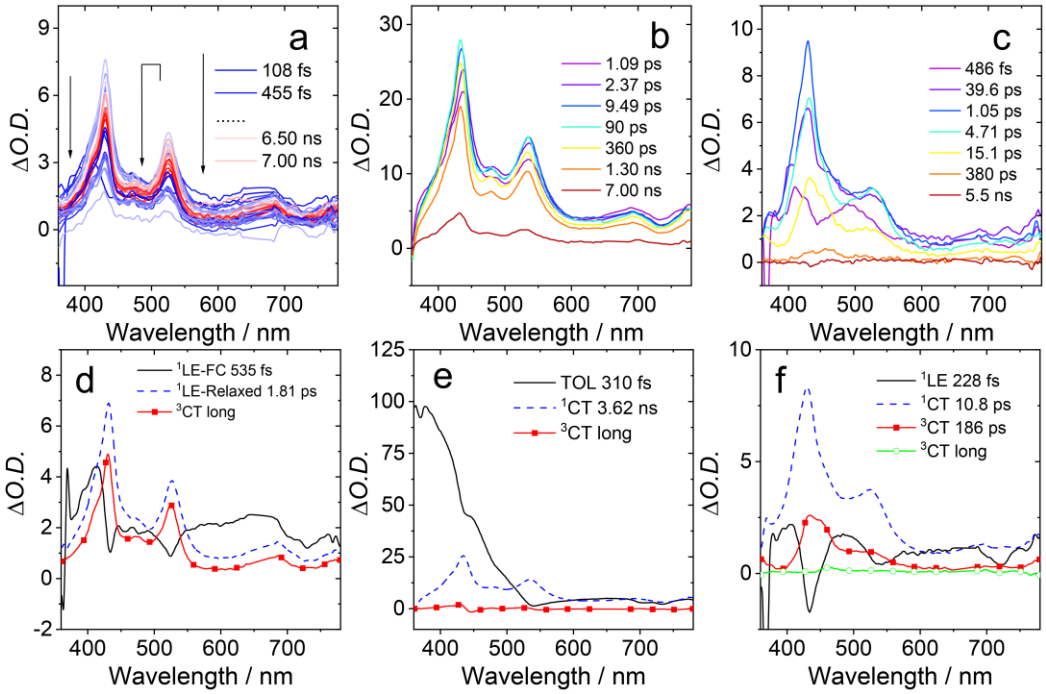

Figure S31. Femtosecond transient absorption spectra of **NI-PXZ-PhOCH$_3$** in (a) HEX, (b) TOL, (c) ACN and relative EADS obtained with global analysis of **NI-PXZ-PhOCH$_3$** in (d) HEX, (e) TOL, (f) ACN. Excited at 330 nm. "FC" stands for Franck–Condon.

11. Calculated by DFT and TDDFT with Gaussian 16

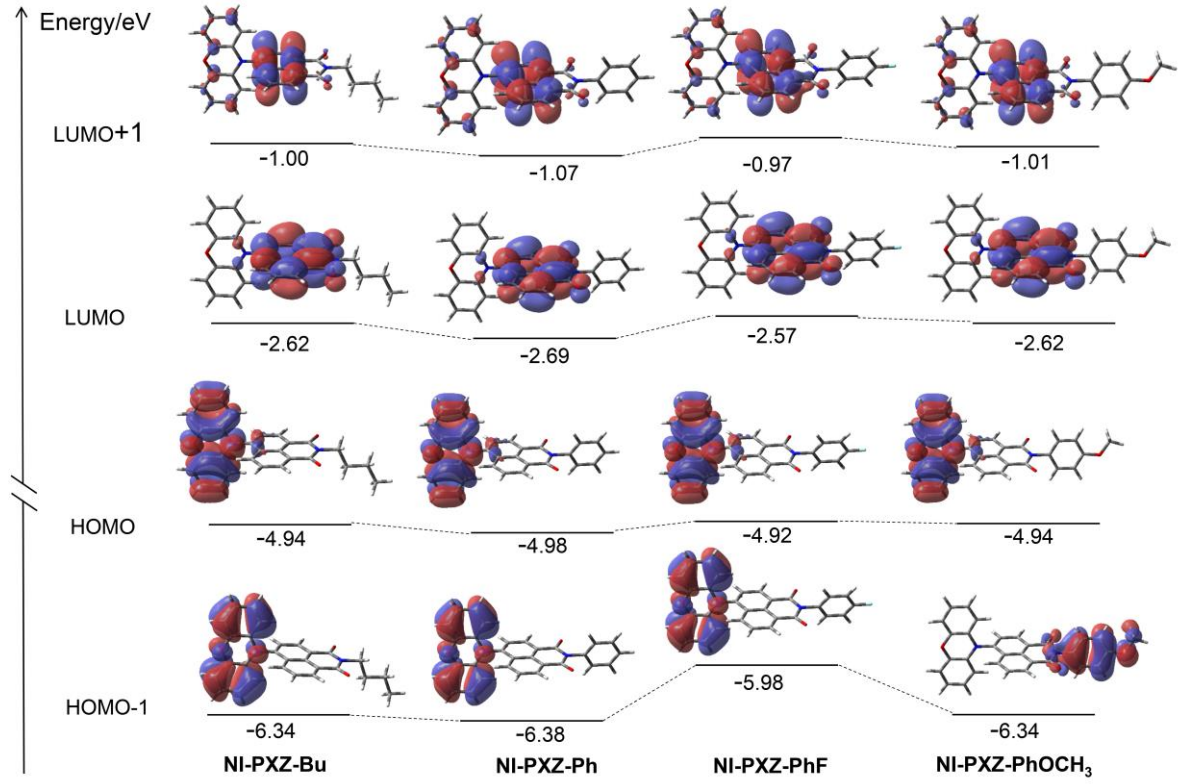

Figure S32. Selected frontier molecular orbitals of **NI-PXZ-Bu**, **NI-PXZ-Ph**, **NI-PXZ-PhF** and **NI-PXZ-PhOCH$_3$** calculated by DFT and TDDFT at the B3LYP/6-31G(d) level with Gaussian 16, based on the optimized ground state and the excited state geometries, unused solvent, respectively (isoval = 0.0004).

12. Computed Electronic Transitions

Table S5. Excitation Energies (eV) and Corresponding Oscillator Strengths (*f*), Main Configurations, and CI Coefficients of the Low-Lying Electronically Excited States of **NI-PXZ-Bu, NI-PXZ-Ph, NI-PXZ-PhF** and **NI-PXZ-PhOCH$_3$**, performed at the B3LYP/6-31G(d) level by using Gaussian09. Based on the DFT//B3LYP Optimized Ground-State Geometries.

	electronic transition	energy [eV / (nm)][a]	*f* [b]	composition[c]	CI [d]	character
NI-PXZ-Bu	$S_0 \rightarrow T_1$	1.69 / 735	0.0000	H→L	0.7037	CT
	$S_0 \rightarrow T_2$	2.29 / 542	0.0000	H−2→L	0.6793	LE
	$S_0 \rightarrow T_3$	2.85 / 435	0.0000	H→L+3	0.5949	LE
NI-PXZ-Ph	$S_o \rightarrow T_1$	1.70 / 731	0.0000	H→L	0.7036	CT
	$S_0 \rightarrow T_2$	2.29 / 541	0.0000	H−2→L	0.6699	LE
	$S_0 \rightarrow T_3$	2.86 / 434	0.0000	H→L+3	0.5946	LE
NI-PXZ-PhF	$S_0 \rightarrow T_1$	1.68 / 738	0.0000	H→L	0.7030	CT
	$S_0 \rightarrow T_2$	2.29 / 542	0.0000	H−3→L	0.6762	LE
	$S_0 \rightarrow T_3$	2.86 / 434	0.0000	H→L+3	0.5929	CT
NI-PXZ-PhOCH$_3$	$S_0 \rightarrow T_1$	1.72 / 722	0.0000	H→L	0.7037	CT
	$S_0 \rightarrow T_2$	2.29 / 541	0.0000	H−3→L	0.6743	LE
	$S_0 \rightarrow T_3$	2.84 / 437	0.0000	H−1→L	0.6904	CT

[a] Only the selected low-lying excited states are presented. [b] Oscillator strengths. [c] TDDFT//B3LYP/6-31G(d)-optimized excited state geometries. [d] Coefficient of the wave function for each excitation. CI coefficients are in absolute values.

13. Reference

[1] X. Zhang, X. Liu, M. Taddei, L. Bussotti, I. Kurganskii, M. Li, X. Jiang, L. Xing, S. Ji, Y. Huo, J. Zhao, M. Di Donato, Y. Wan, Z. Zhao, M. V. Fedin, *Chem. Eur. J.*, 2022, **28**, e202200510.

[2] F. Ye, X.-M. Liang, K.-X. Xu, X.-X. Pang, Q. Chai, Y. Fu, *Talanta*, 2019, **200**, 494–502.

[3] S. Jena, P. Dhanalakshmi, G. Bano, P. Thilagar, *J. Phys. Chem. B.* 2020, **124**, 5393−5406.